ARTICLE

# Predicting the retention time of microparticles in electrokinetic migration

Received 00th January 20xx,
Accepted 00th January 20xx

DOI: 10.1039/x0xx00000x

Alaleh Vaghef-Koodehi,[a] Victor H. Perez-Gonzalez,*[b] and Blanca H. Lapizco-Encinas*[a]

Insulator based electrokinetic (iEK) devices have emerged as powerful tools for analyzing both nano- and microparticles due to their simplicity, robustness, and ability to integrate linear and nonlinear electrokinetic (EK) effects into a single platform. Recent studies emphasize the importance of nonlinear electrophoresis ($EP_{NL}$) in particle analysis, for performing separations based on size, shape, and charge differences. Despite these advancements, the development of an empirical equation for predicting particle retention times in iEK-based systems that incorporates $EP_{NL}$ remains limited. This study presents a method for predicting particle retention time in iEK systems in scenarios where the linear EK regime allows for particles migration, while also incorporating $EP_{NL}$ and accounting for particle characteristics, applied electric fields, and microdevice features. Experiments were conducted using eight reference microparticles, grouped into four pairs with similar sizes (3.6 µm to 11.7 µm) but distinct zeta potentials (~-20 mV and ~-30 mV), across three distinct iEK microdevices: one with asymmetrical oval-diamond posts, one with symmetrical oval posts, and one postless design. Experimental retention times ($t_{R,e}$) were measured at applied voltages ranging from 400 V to 1450 V. Using the collected $t_{R,e}$ data, three empirical equations were developed to describe particle velocity, incorporating both linear and nonlinear velocities. Validation with two control particles demonstrated prediction errors below 24% in all devices. These findings underscore the potential of the empirical equations in predicting particle behavior in iEK systems.

## Introduction

Various conventional techniques such as capillary electrophoresis (CE) and chromatography are accessible for the analysis of nano-sized bioparticles, yet there is a scarcity of equally effective methods for analyzing micron-sized particles, such as microorganisms.[1] Microfluidic systems have proven successful in investigating both nano- and micro- particles.[1–3] Within the realm of microfluidics, electrokinetic (EK) techniques play a significant role in analyzing particles. Specifically, insulator based EK (iEK) systems have garnered attention recently due to their simplicity, robustness, and unique ability to merge linear and nonlinear EK effects within a single microfluidic device.[4,5] In these systems, insulating structures integrated into microchannels modify the distribution of the externally generated electric field, leading to the creation of zones with higher electric field intensity that enable nonlinear EK effects therein, whereas only linear EK effects dictate particle dynamics in the remaining zones. The utilization of iEK devices has facilitated the separation of complex samples, encompassing bioparticles ranging from macromolecules to mammalian cells.[6–10]

Numerous research groups have utilized iEK systems to analyze particles and cells based on differences in size and/or charge.[11–13] Nevertheless, previous studies overlooked the inclusion of nonlinear electrophoresis ($EP_{NL}$), also referred to as EP of the second kind, necessitating the use of empirically-determined correction factors to reconcile experimental and predicted outcomes.[14]

Recent reports revealed the importance of $EP_{NL}$ in iEK systems.[15–17] Employing $EP_{NL}$ allows separations by exploiting shape and size differences, which are not possible with traditional methods, such as linear electrophoresis ($EP_L$).[18,19] Several recent studies by our group[20–28] have integrated COMSOL *Multiphysics* simulations and experimental validation to predict and confirm particle and cells retention times ($t_R$) in iEK systems. The charge-based separation of almost similar polystyrene analytes[20], the binary separation of cells[21,22], tertiary separation of particles[24] under DC voltages, the utilization of different input voltages to transition between linear and nonlinear electrokinetic regimes[23], and EK separation experiments employing DC-biased AC voltages[27] highlight the importance of $EP_{NL}$ in particle analysis. These efforts feature the criticality of accurately predicting the time it takes a given particle type to migrate through the microchannel, known as particle retention time, to optimize performance and expand the applicability of iEK systems.

Building on the understanding of the importance of $EP_{NL}$, a practical approach to further enhance the efficiency of iEK

[a] *Microscale Bioseparations Laboratory and Biomedical Engineering Department, Rochester Institute of Technology, 160 Lomb Memorial Drive, Rochester, New York, 14623, United States.*
[b] *Tecnologico de Monterrey, School of Engineering and Sciences, Ave. Eugenio Garza Sada 2501 Sur, Col: Tecnológico, Monterrey, N.L., México, 64700. E-mail: vhpg@tec.mx*

† Electronic supplementary information (ESI) available: Predicting retention time of microparticles in electrokinetic separations. See DOI: 10.1039/x0xx00000x

systems is to develop empirical equations for predicting particle retention time. Such empirical equations enable rapid estimation of system behavior, conserving both time and resources. For instance, the Van Deemter equation in chromatography employs factors such as diffusion and mass transfer kinetics to relate the variance per unit length of a separation column to the linear mobile phase velocity[29].

This study presents a novel approach to predicting particle retention time, based on key factors such as particle characteristics, applied voltages, and microdevice design features. Eight distinct types of microparticles, grouped into four pairs, were investigated to evaluate the proposed model's applicability. Each pair consisted of particles with nearly identical sizes ranging from 3.6 µm to 11.7 µm but differing zeta potentials, approximately -20 mV and -30 mV. The experiments were performed using three distinct microdevice configurations: two devices with insulating posts—one featuring asymmetrical posts and the other with symmetrical posts—and a postless device serving as a control. Particle velocities and retention times were systematically measured at eight applied DC voltages, ranging from 400 V to 1450 V. Within this range, a linear regime allows particles to move through the channel without being trapped by the non-negligible effects of $EP_{NL}$ present during the experiments as demonstrated by our previous studies.[23]

The experimental retention time data was used to derive three empirical correlation equations that describe particle velocity as a function of both linear and nonlinear EK velocity components for each device. These equations offer insights into the dynamics of particle migration under varying electric field conditions. To validate the proposed model, two control particles were tested across the three devices. The three empirical equations produced retention time predictions with errors remaining below 24%, underscoring the effectiveness of the proposed approach for rapidly predicting particle behavior in electrokinetic systems. Notably, while other studies[30] have required correction factors larger than 100 to account for all phenomena present in similar systems (i.e., correcting prediction errors greater than 10,000%), our model achieved satisfactory predictions without such extensive corrections, making the 24% error particularly encouraging. These correlations can become valuable tools in the design of new separation processes, advancing microfluidic applications in biomedical and analytical research.

## Theory

Electrokinetic phenomena are categorized based on their reliance on the electric field, as linear and nonlinear. The linear EK phenomena considered in this study are electroosmosis (EO) and linear electrophoresis ($EP_L$). The velocities expressions of these phenomena are stated below:[3,4,31]

$$\mathbf{v}_{EO} = \mu_{EO}\mathbf{E} = -\frac{\varepsilon_m \zeta_W}{\eta}\mathbf{E} \quad (1)$$

$$\mathbf{v}_{EP,L} = \mu_{EP,L}\mathbf{E} = \frac{\varepsilon_m \zeta_P}{\eta}\mathbf{E} \quad (2)$$

$$\mathbf{v}_{EK} = \mathbf{v}_{EO} + \mathbf{v}_{EP,L} = \mu_{EK}\mathbf{E} \quad (3)$$

where $\mathbf{v}$ is velocity, $\mu$ stands for mobility, $\varepsilon_m$ and $\eta$ define the permittivity and viscosity of the suspending medium, respectively, $\zeta$ is the zeta potential for either the channel wall or the microparticle, and $\mathbf{E}$ is the electric field with magnitude $E$ and direction $\hat{\boldsymbol{a}}_{\boldsymbol{E}}$. While the presence of nonlinear electroosmosis ($EO_{NL}$) is acknowledged, it is considered negligible in this study due to the extremely small electrical double layer (EDL) thickness of 14 nm on the surface of the PDMS devices. Instead, the focus is on nonlinear EK phenomena, specifically dielectrophoresis (DEP) and nonlinear electrophoresis ($EP_{NL}$). One significant advantage of $EP_{NL}$ compared to $EP_L$ is its capability to discriminate based on the size or shape of the target analytes, thereby enabling separations that are not attainable with $EP_L$ alone.[18,19] The velocity equations for $EP_{NL}$ and DEP are as follows:[3,4,31]

$$\mathbf{v}_{EP,NL}^{(3)} = \mu_{EP,NL}^{(3)} E^3 \hat{\boldsymbol{a}}_{\boldsymbol{E}} \quad (4)$$

moderate field regime which occurs at $\beta \leq 1$, arbitrary *Du*, and $Pe \ll 1$

$$\mathbf{v}_{EP,NL}^{(3/2)} = \mu_{EP,NL}^{(3/2)} E^{3/2} \hat{\boldsymbol{a}}_{E} (5)$$

strong field regime which occurs at $\beta > 1$, $Du \ll 1$, and $Pe \gg 1$

$$\mathbf{v}_{DEP} = \mu_{DEP}\nabla E^2 = \frac{r_p^2 \varepsilon_m}{3\eta}\mathrm{Re}[f_{CM}]\nabla E^2 \quad (6)$$

where $r_p$ signifies the particle radius; Re[$f_{CM}$] shows the real part of the Clausius-Mossotti factor, which defines particle polarization in a given suspending medium; $\mu_{EP,NL}^{(3)}$ and $\mu_{EP,NL}^{(3/2)}$ are the mobilities of the $EP_{NL}$ velocity for the models with $E^3$ and $E^{3/2}$ dependencies, respectively; $\beta$ is dimensionless applied field strength coefficient; *Du* is Dukhin number; and $Pe$ is Peclet number. The defining expressions for these numbers can be found in the supplementary information (SI) document. It is worth mentioning that while **Eq. 4** and **Eq. 5** do not explicitly illustrate size or shape dependence, the influence of these parameters on nonlinear electrophoretic mobility, $\mu_{EP,NL}^{(n)}$, has been demonstrated in the literature.[32–34] Considering these four EK phenomena, the overall particle velocity ($\mathbf{v}_P$) becomes:

$$\mathbf{v}_P = \mathbf{v}_{EK} + \mathbf{v}_{DEP} + \mathbf{v}_{EP,NL}^{(n)} = \mu_{EK}\mathbf{E} + \mu_{DEP}\nabla E^2 + \mu_{EP,NL}^{(n)} E^n \hat{\boldsymbol{a}}_{\boldsymbol{E}} \quad (7)$$

The overall particle velocity in the iEK microchannel (**Fig. 1**) is determined by EK phenomena illustrated in **Fig. 1a** in the postless device and **Fig. 1b** in post devices for negatively charged particles. Given that the DEP force in our system is negligible[16,17,31,35] and the 3/2 condition is either not met or occurs only in negligibly small regions based on the applied voltage (as detailed in **Table S1**), the equation can be simplified as follows:

$$\mathbf{v}_P = \mathbf{v}_{EK} + \mathbf{v}_{EP,NL}^{(3)} = \mu_{EK}\mathbf{E} + \mu_{EP,NL}^{(3)} E^3 \hat{\boldsymbol{a}}_{\boldsymbol{E}} \quad (8)$$

**Table 1**. Characteristics of the microparticles used in this study.

| Particle ID | Diameter (μm) | $\zeta_{P}$§ (mV) | $\mu_{EP,L}$x10$^{-8}$ (m$^2$V$^{-1}$s$^{-1}$) | E for $\mu_{EP,NL}^{(3)}$ estimation (V/cm) | $\beta$ for $\mu_{EP,NL}^{(3)}$ estimation | *Pe* for $\mu_{EP,NL}^{(3)}$ estimation | $\mu_{EP,NL}^{(3)}$x10$^{-18}$ (m$^4$V$^{-3}$s$^{-1}$) |
|---|---|---|---|---|---|---|---|
| P1 | 3.6 ± 0.1 | -19.1 ± 3.2 | -1.5 ± 0.2 | 350 | 3.3 | 0.8 | -2.1 ± 0.3 |
| P2 | 4.1 ± 0.3 | -34.1 ± 2.5 | -2.6 ± 0.1 | 250 | 2.8 | 1.1 | -3.1 ± 0.3 |
| P3 | 5.8 ± 0.2 | -20.5 ± 2.2 | -1.6 ± 0.2 | 150 | 1.1 | 0.2 | -25.3 ± 2.5 |
| P4 | 5.7 ± 0.2 | -34.2 ± 3.3 | -2.7 ± 0.1 | 150 | 2.2 | 0.9 | -16.1 ± 1.1 |
| P5 | 7.4 ± 0.3 | -21.1 ± 1.6 | -1.6 ± 0.1 | 100 | 1.9 | 0.5 | -25.3 ± 2.3 |
| P6 | 7.6 ± 0.2 | -26.7 ± 1.8 | -2.1 ± 0.2 | 100 | 1.9 | 0.6 | -16.4 ± 1.7 |
| P7 | 11.7 ± 0.2 | -23.8 ± 1.1 | -1.9 ± 0.8 | 100 | 2.9 | 0.9 | -23.2 ± 1.6 |
| P8 | 10.5 ± 0.3 | -27.8 ± 4.6 | -2.2 ± 0.3 | 100 | 2.7 | 0.9 | -19.8 ± 1.1 |
| P9 | 3.6 ± 0.1 | -20.7 ± 2.7 | -1.6 ± 0.2 | 300 | 2.4 | 1.2 | -20.5 ± 3.0 |
| P10 | 7.4 ± 0.3 | -31.7 ± 1.8 | -2.5 ± 0.1 | 100 | 1.9 | 0.7 | -7.3 ± 0.6 |

§ The values for the $\zeta_P$ and $\mu_{EP,L}$ were estimated at $\beta$ values between 0.2 and 0.9.

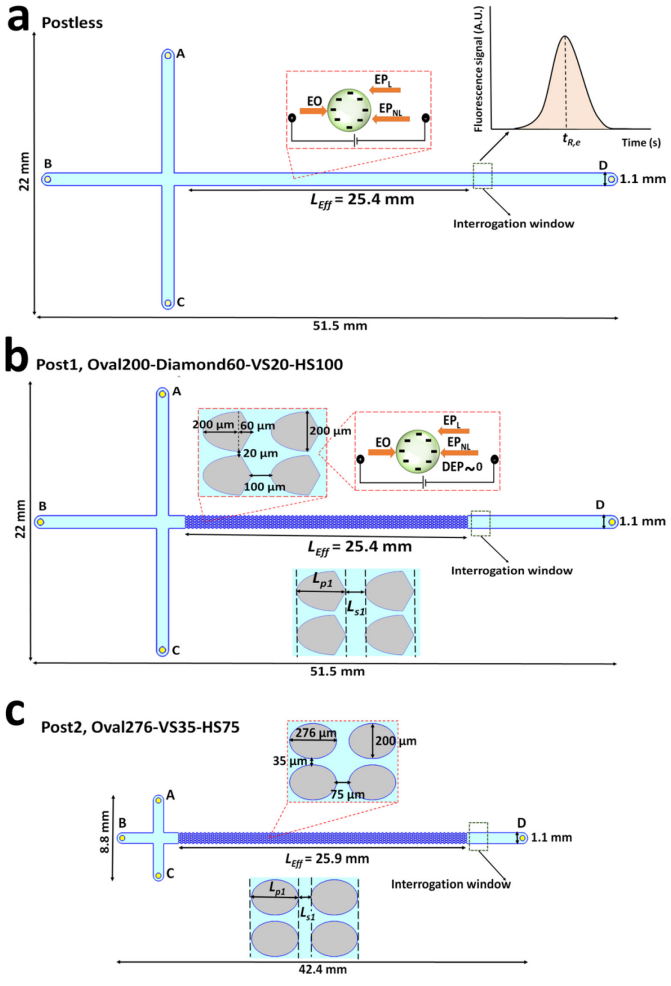


**Fig. 1** Illustration of the three device designs employed in this study. Schematic representation of **(a)** a postless microchannel, **(b)** a microchannel with asymmetrical posts (Post1 device), **(c)** a microchannel with symmetrical posts (Post2 device) with reservoirs, depicting the channel dimensions, and the interrogation window used for fluorescence measurements. The labels A–D refer to the four electrodes (see **Table 2**). The EK forces (EO, EP$_L$, EP$_{NL}$, and DEP) acting on the negatively charged particles in the microchannels are also shown in the figure inset in (a) and (b). Because the DEP force is negligible in magnitude when compared to the other EK forces, it is shown as DEP∼0 in (b). The insets below the channels in (b) and (c) provide an illustration of the effective length ($L_{Eff}$) the length of one horizontal gap between posts ($L_{s1}$) and the length of one post ($L_{p1}$) for the post devices. The second inset in **(a)** illustrates where retention time data is obtained in an electropherogram.

## Experimental

### Suspending medium and microparticles

This study utilized eight distinct types of polystyrene microparticles as reference particles (P1 to P8, as detailed in **Table 1**) sourced from Magsphere (Pasadena, CA, USA) and Spherotech (Lake Forest, IL, USA) with sizes ranging from 3.6 μm to 11.7 μm to develop the empirical equations. The particles were grouped into four pairs, each consisting of microparticles of nearly identical size but differing zeta potentials, approximately -20 mV and -30 mV. Additionally, two particles, referred to as control particles, were used to validate the empirical equations. One particle had a smaller size of 3.6 μm (particle P9), and the other had a larger size of 7.4 μm (particle P10). Both particles had characteristics within the range defined bythe reference particles. The characteristics of particles P9 and P10 are detailed in **Table 1**. The concentration of particles ranged from $\sim 2 \times 10^6$ to $\sim 2 \times 10^8$ beads/ml. The sample concentration was kept consistent across both particle tracking velocimetry (PTV) and EK migration experiments; however, larger sample volumes were required for the EK migration experiments to aid in the visualization of eluting particles.

The suspending media was a buffer solution of $K_2HPO_4$ (Solon, Ohio, USA) at a 0.2 mM concentration, with the addition of 0.05% (v/v) of Tween 20 (Solon, Ohio, USA) to prevent particle sticking. The media had a conductivity of 41 ± 3.0 μS/cm with a pH of 7.2 ± 0.5, which produced a wall zeta potential ($\zeta_W$) of -60.1 ± 3.7 mV and $\mu_{EO}$ of 4.7 ± 0.3 x 10$^{-8}$ m$^2$V$^{-1}$s$^{-1}$ as measured with current monitoring.

**Table 2.** Voltage conditions used for EK sample injection.

| Device | Step | Run time (s) | Applied voltage (V) in each reservoir | | | |
|---|---|---|---|---|---|---|
| | | | A | B | C | D |
| Postless & Post1 | Loading | 10 | 1500 | 100 | 0 | 1000 |
| | Gating | 2 | 1500 | 2500 | 1500 | 0 |
| Post2 | Loading | 10 | 800 | 100 | 0 | 1000 |
| | Gating | 2 | 1500 | 2500 | 1500 | 0 |
| | Injection | $\ddot{t}$ | 200 | $\ddot{V}_{in}$ | 200 | 0 |

- The values of $\ddot{t}$ vary depending on applied voltage (100 s to 300 s).

- The values of $\ddot{V}_{in}$ vary depending on applied voltage (400 V: 150 V: 1450 V).

**Microdevices and equipment**

Standard cast-molding techniques were employed to create the T-channel devices used in this study.[36] **Fig. 1a-1c** represent the three microchannel designs, with a depth of 40 µm, used in this study; depicting insulating posts and channel dimensions, and the location of the fluorescence interrogation window. The labels A–D refer to the four electrodes (**Table 2**). The insulating posts were chosen to include one asymmetrical (Post1, Oval200-Diamond60-VS20-HS100) and one symmetrical (Post2, Oval276-VS35-HS75) design, as these are among the most commonly used shapes in iEK migration experiments and produce distinct electric field patterns.[23,27] The design names are structured to comprise the shape of the asymmetric/symmetric posts along with their specific horizontal lengths, followed by the vertical spacing (VS) and horizontal spacing (HS) values. In addition to both device designs featuring different post geometries, the shorter arm of Post2 further modifies the electric field intensity in comparison to Post1, allowing for a meaningful comparison of retention times between the two. A postless device was selected as a reference to enable direct comparison with devices containing posts. To minimize the impact of PDMS aging on $\zeta_W$ all microdevices used in this study were 1–2 days old.[37] The effective length ($L_{Eff}$) is fixed at approximately 2.5 cm, with post devices selected accordingly for retention time comparison, and the postless design includes a distance-marking feature above the channel to visually indicate the 2.5 cm endpoint during video recording. All experiments were recorded employing either of two inverted microscopes, a Zeiss Axiovert 40 CFL and a Leica DMi8. The Zeiss Axiovert 40 CFL microscope was used for the EK migration experiments, while both the Zeiss Axiovert 40 CFL and Leica DMi8 microscopes were used for the PTV experiments. A LabSmith high-voltage power supply (model HVS6000D) was used to apply the voltage sequences to the microchannels.

**Experimental procedure**

Experimental work was carried out in two parts: (1) PTV experiments were conducted a 1-cm long postless channel to characterize the particles as reported in **Table 1**. (2) Electrokinetic migration experiments were performed to obtain the retention time of particles ($t_{R,e}$) within the effective length of microchannels. For all experiments, the microchannels were pre-filled with the suspending medium and allowed to equilibrate for at least 12 hours to ensure stable electroosmotic flow. Low-voltage PTV experiments, using applied voltages ranging from 25 to 75 V, were performed to obtain values for $\mu_{EP,L}$, which were then used to determine $\zeta_P$. These low voltage magnitudes were selected to ensure that *Pe* and $\beta$ remained much smaller than 1, maintaining a linear relationship with $\mathbf{E}$. High-voltage PTV experiments were carried out at higher voltages to collect nonlinear electrophoretic data ($\mu^{(3)}_{EP,NL}$) to satisfy moderate condition where $Pe \ll 1$, arbitrary $Du$, and $\beta \leq 1$. **Table 1** presents the values of $\beta$ and *Pe* used for estimating linear and nonlinear mobilities. Although these are not the exact values required, they represent the closest available approximations. A detailed description of the PTV experiments can be found in our previous reports.[34,38,39] To obtain $t_{R,e}$, electrokinetic migration experiments were performed employing a three-step EK sample injection process: loading, gating, and injection. The applied voltages in the injection step range from 400 V to 1450 V with an increment of 150 V (see **Table 2**). The voltage range was set between 400 V, the minimum required for EK injection, and 1450 V, the maximum at which particles can migrate within the channel while being affected (but not trapped) by $EP_{NL}$ effects. The run time refers to the duration of each voltage step; the duration of the injection step was determined by the time required for the particles to elute from the post array. Large liquid reservoirs (~3-4 mL) were employed to decrease pressure-driven backflow. A 1-6 µL suspension of microparticles was introduced into reservoir A (shown in **Fig. 1**) using a pipette, followed by the placement of platinum wire electrodes into each of the four reservoirs. These experiments are thoroughly described in our earlier publications.[20,21] The EK injection experiments were conducted at least three times for each particle at each voltage to ensure reproducibility. The fluorescence signal from each eluting particle peak was captured at the interrogation window shown in **Fig. 1**. EK migration videos were recorded and analyzed using ImageJ, which processed the videos based on fluorescence intensity. The fluorescence intensity for each EK migration video was quantified using the first frame of the interrogation window as a threshold. To ensure consistency, intensity values were normalized relative to the highest recorded intensity. The second inset in **Fig. 1a** represents an electropherogram generated from fluorescence analysis at the interrogation window, illustrating the $t_{R,e}$ in a single elution peak. $t_{R,e}$, along with the standard deviations from these repetitions, are presented in **Tables S2–S4** for different voltages and across three microfluidic devices.

**Data fitting**

The "*lsqnonlin*" function in MATLAB R2024a was used to fit the experimental retention time data to the proposed model. This function optimizes the parameters by minimizing the sum of squared residuals between the predicted and observed values. Its flexibility in handling bounds and constraints made it particularly suitable for accurately modeling the nonlinear relationships in the system. Since the retention time of particles is determined by their overall velocity, which is the summation of the $\mathbf{v}_{EK}$ and $\mathbf{v}^{(3)}_{EP,NL}$, the equation for particle retention time can be expressed based on particles' linear ($\mu_{EK}$) and nonlinear

 

($\mu_{EP,NL}^{(3)}$) mobilities as shown in **Eq. 8**. Mobility is a key parameter in the proposed model because it effectively captures the system's physical behavior and is relatively straightforward to characterize, as demonstrated by a recent report.[40] The average of electric fields ($\mathbf{E}_{Avg}$) along a cutline (**Fig. S2**) was calculated using COMSOL *Multiphysics* and employed in the fitting process. This approach was chosen because of our observations of particles primarily migrating and aligning along the cutline rather than across the entire volume. In COMSOL, the Average tool computes the average electric field by integrating the field values over the length of the line and dividing by the total length. **Table S7** presents the $\mathbf{E}_{Avg}$ values across the cutlines for all devices. Detailed information about the computational modeling is provided in the Supporting Information (**Figs S1–S2** and **Tables S5–S6**). In this study, the experimental retention time data ($t_{R,e}$), as reported in **Tables S2–S4**, were individually fitted for the postless, Post1, and Post2 devices to derive three distinct equations for the predicted retention time of particles ($t_{R,p}$). For the postless device, **Eq. 8** was reformulated as follows:

$$\mathbf{v}_P = A_1\,\mu_{EK}\,\mathbf{E}_{Avg} + A_2\,\mu_{EP,NL}^{(3)}\,\mathrm{E}_{Avg}^3\widehat{\boldsymbol{a}}_{\boldsymbol{E}} \tag{9}$$

$$t_R = \frac{L_{Eff}}{v_P} = \frac{L_{Eff}}{A_1\,\mu_{EK}\,E_{Avg} + A_2\,\mu_{EP,NL}^{(3)}\,E_{Avg}^3} \tag{10}$$

where $t_R$ is the retention time of particles in the migration channel, $v_P = L_{Eff}/t_R$, $L_{Eff}$ denotes the effective length of the migration channel and is shown in **Fig. 1a**. $A_1$ represents the coefficient for the linear electrokinetic term ($\mathbf{v}_{EP,L}$), while $A_2$ corresponds to the coefficient for the $\mathbf{v}_{EP,NL}^{(3)}$ term. The coefficients of $A_1$ and $A_2$ represent a weight for the overestimation or underestimation associated with the linear and nonlinear regimes and should always remain positive to preserve the physical meaning of both terms. $\mathbf{E}_{Avg}$ is the average of the electric field in $L$ calculated by COMSOL, reported in **Table S7**.

Similarly, the equation can be adapted for post devices by accounting for the average electric field in the presence of the insulating posts:

$$\mathbf{v}_P = A_1\,\mu_{EK}\,\left(\frac{L_s}{L_{Eff}}\,\mathbf{E}_{Avg,Ls} + \frac{L_p}{L_{Eff}}\,\mathbf{E}_{Avg,Lp}\right) + A_2\,\mu_{EP,NL}^{(3)}\,\frac{L_p}{L_{Eff}}\left(\mathrm{E}_{Avg,Lp}^3\widehat{\boldsymbol{a}}_{\boldsymbol{E}}\right) \tag{11}$$

$$L_{Eff} = L_s + L_p \tag{11a}$$

$$L_s = (N_c + 1)\,(L_{s1}) \tag{11b}$$

$$L_p = (N_c)\,(L_{p1}) \tag{11c}$$

$$t_R = \frac{L_{Eff}}{A_1\,\mu_{EK}\,\left(\frac{L_s}{L_{Eff}}E_{Avg,Ls} + \frac{L_p}{L_{Eff}}E_{Avg,Lp}\right) + A_2\,\mu_{EP,NL}^{(3)}\,\frac{L_p}{L_{Eff}}\left(E_{Avg,Lp}^3\right)} \tag{12}$$

where $L_{Eff}$ represents the length of the post array, $L_{s1}$ is the length of one horizontal gap between posts, $L_{p1}$ is the length of one post, $N_c$ is the number of columns in the post array. For Post1 device $N_c = 71$ and for Post2 device $N_c = 75$. The ratios of $L_s/L_{Eff}$ and $L_p/L_{Eff}$ act as weights, guiding the equation to accurately represent the distribution of the electric fields. For post devices, $L_{Eff}$, $L_{s1}$, and $L_{p1}$ are illustrated in **Fig. 1b-1c**. $E_{Avg,Ls}$ is the average of electric field in $L_s$, and $E_{Avg,Lp}$ is the average of electric field in $L_p$ which are reported in **Table S7** .

## Results and discussion

## The experimental retention time of particles

This study developed empirical equations using eight types of polystyrene microparticles (P1 to P8, as shown in **Table 1**) to predict the retention time in microfluidic devices, with experiments conducted on three microdevice types (shown in **Fig. 1a-1c**). The retention times of the particles, together with their standard deviations from repeated measurements, are provided in **Tables S2-S4** for various voltages and three different microfluidic devices. **Fig. 2a-2h** presents the experimental retention time of the microparticles in the three microfluidic devices, represented by markers with error bars. The model-predicted retention times are shown as solid lines, demonstrating a reasonable agreement with the experimental data. Across all devices, the relative error between $t_{R,e}$ and $t_{R,p}$ remains below 30% for all particles. A descending trend is observed for all particles across all devices as the applied voltage increases, except for a slight increase at higher voltages (reported in **Tables S2-S4**).

The retention time of particles is influenced by a combination of linear and nonlinear effects. As detailed in **Tables S2-S4**, at lower voltages (400-700 V), where linear forces are more pronounced, the retention time decreases noticeably with increasing voltage, as expected. As the voltage increases to the mid-range (700-1000 V), the retention time decreases at a lower rate, and in some case retention time increases at the higher voltages (1000-1200 V), suggesting that $EP_{NL}$ effects counteract linear forces. Eventually, an increase in retention time is observed, likely due to the growing influence of nonlinear forces which are becoming comparable to linear effects. This trend, which is more obvious in Post1 device, underscores the complex interaction between linear and nonlinear phenomena at varying voltage levels. The performance of post devices in terms of producing longer retention times, considering $EP_{NL}$, is expected to become more significant at higher voltages, as demonstrated in our previous work.[23] However, due to concerns about particle trapping for larger particles, the voltage was not increased to that level.

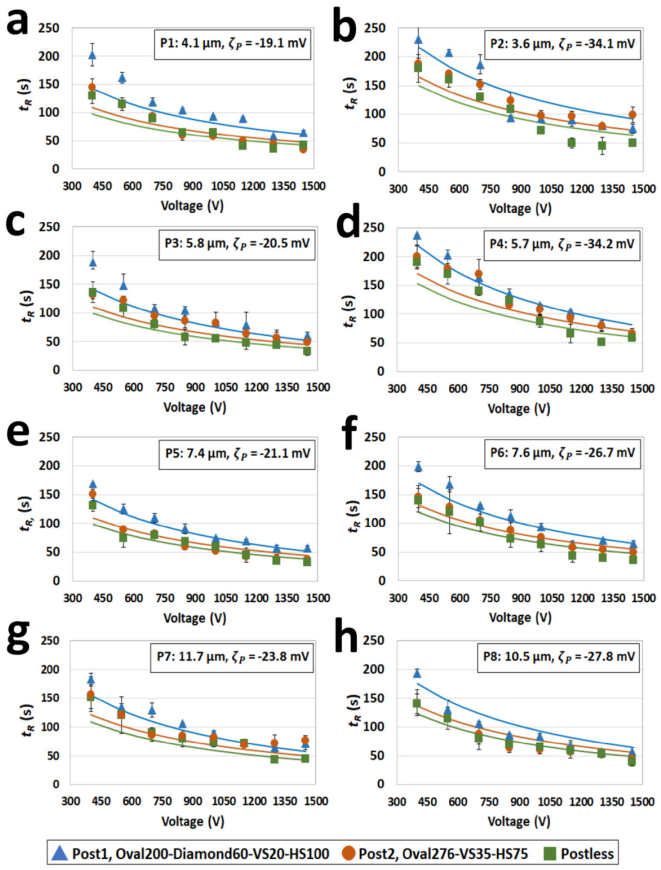


**Fig. 2 (a-h)** Experimental retention times ($t_{R,e}$, markers) and model predictions ($t_{R,p}$, solid lines) for reference particles P1–P8 as a function of applied voltage (400 V to 1450 V) for three device configurations: Post1 (Oval200-Diamond60-VS20-HS100), Post2 (Oval276-VS35-HS75), and postless. The retention times decrease consistently with increasing voltage across all devices, with variations between device types. Error bars represent the standard deviations from repetitions at each voltage, indicating the reliability of the measurements.

The results revealed that, in general, the Post1 device (Oval200-Diamond60-VS20-HS100) produced longer retention times compared to the other two devices. Additionally, the Post2 device (Oval276-VS35-HS100) generally resulted in longer retention times than the postless device, although not to the extent of the Post1 device. On average, the Post1 device extended retention times by ~40% (95% CI: 20% to 60%) compared to the postless device, while the Post2 device demonstrated a ~20% increase (95% CI: 3% to 37%) in retention times relative to the postless configuration. These observations can be explained by electric field distributions and the magnitude of $EP_{NL}$ within the devices. In the postless device, the electric field distribution is uniform, which limits the emergence of $EP_{NL}$ compared to post devices. In postless device, particles can move more quickly toward the outlet, resulting in shorter $t_{R,e}$. In contrast, insulating features intensify the magnitude of the electric fields at certain regions of the channel, enabling the simultaneous utilization of both linear and nonlinear electrokinetic phenomena within the post device, making the particle move slower toward the outlet and obtain longer $t_{R,e}$. Furthermore, asymmetrical insulating posts (Post1 device) more effectively amplify the effects of $EP_{NL}$ on particles exposed to the electric field compared to symmetrical posts (Post2 device), as evident in the plots and consistent with the literature.[14,36]

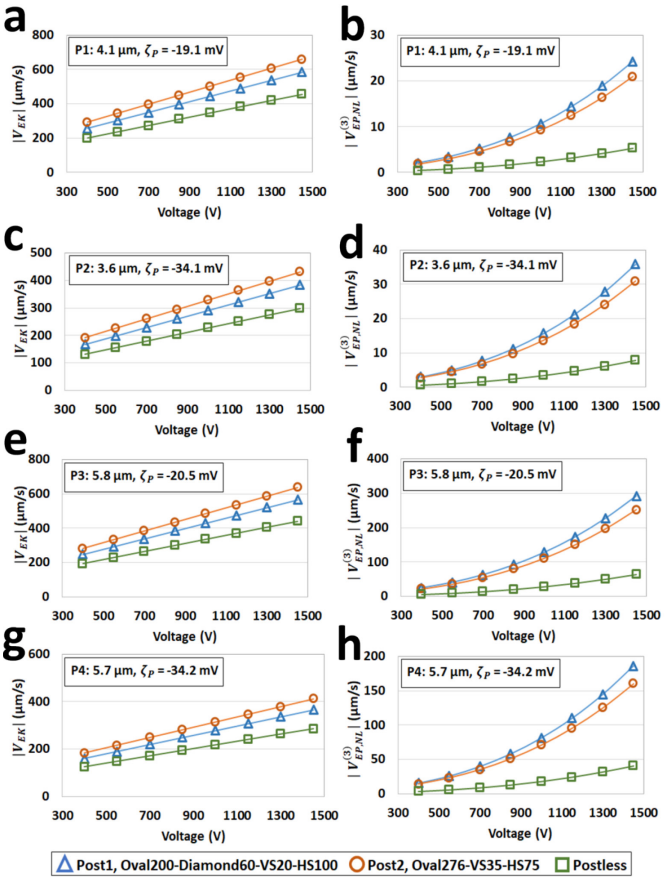


**Fig. 3** Predicted electrokinetic velocities $|\mathbf{v}_{EK}|$ and the nonlinear velocity term ($|\mathbf{v}^{(3)}_{EP,NL}|$), for particles P1–P4 as a function of applied voltage, derived from empirical equations for three device configurations: Post1 (Oval200-Diamond60-VS20-HS100), Post2 (Oval276-VS35-HS75), and postless. **(a, c, e, g)** Plots of $|\mathbf{v}_{EK}|$ vs. Voltage for particles P1, P2, P3, and P4. **(b, d, f, h)** Plots of $|\mathbf{v}^{(3)}_{EP,NL}|$ vs. Voltage for the same particles. The absolute values of predicted $\mathbf{v}^{(3)}_{EP,NL}$ were plotted to aid visualization, since all $\mu^{(3)}_{EP,NL}$ values are negative for all particles in this study. The results highlight the differences in $\mathbf{v}_{EK}$ and $\mathbf{v}^{(3)}_{EP,NL}$ across devices and demonstrate how particle size and zeta potential influence the trends.

## Development of empirical equations for predicting particle retention time

The experimental retention times of particles ($t_{R,e}$) across various devices and applied voltage ranges were utilized to develop an empirical equation for predicting particle retention time ($t_{R,p}$) based on linear and nonlinear velocities. The equation for the postless device was fitted using the format specified in **Eq. 10**, while the equations for the Post devices adhered to the format outlined in **Eq. 12**. The solver determined the equation parameters using $t_{R,e}$ as the response variable in the postless device. This resulted in coefficients $A_1$ = 1.31 and $A_2$ = 1.32, corresponding to the contribution of $\mathbf{v}_{EP,L}$ and $\mathbf{v}_{EP,NL}$, respectively. It is important to note that $L_{Eff}$ must be provided in meters and $E_{Avg}$ in volts per meter (V/m) for these equations to function correctly. For the postless

device, given that $L_{Eff} = 0.025\ m$, the resulting equation is as follows:

$$t_{R,p} = \frac{0.025}{1.31\ \mu_{EK}\ E_{Avg} + 1.32\ \mu_{EP,NL}^{(3)}\ E_{Avg}^3} \quad (13)$$

For the Post1 device, the solver estimated the equation parameters by using $t_{R,e}$ obtained from Post1 device as the response variable. Knowing that $L_{Eff} = 0.025$, $L_s/L_{Eff} = 0.3$, and $L_p/L_{Eff} = 0.7$, this process yielded coefficients $A_1$ = 0.63 and $A_2$ = 0.32, which correct the estimation of linear electrokinetic effects and nonlinear phenomena, respectively. The equation derived for the Post1 device is expressed as follows:

$$t_{R,p} = \frac{0.025}{0.63\ \mu_{EK}\ (0.3\ E_{Avg,Ls} + 0.7\ E_{Avg,Lp}) + 0.32\ \mu_{EP,NL}^{(3)}\ (0.7\ E_{Avg,Lp}^3)} \quad (14)$$

In the Post2 device given that $L_{Eff} = 0.026$, $L_s/L_{Eff} = 0.2$, and $L_p/L_{Eff} = 0.8$, the model estimated the equation parameters by employing $t_{R,e}$ obtained from Post2 device as the response variable. This process yielded coefficients $A_1$ = 0.83 and $A_2$ = 0.22. For the Post2 device, the resulting equation can be represented as:

$$t_{R,p} = \frac{0.026}{0.83\ \mu_{EK}\ (0.2\ E_{Avg,Ls} + 0.8\ E_{Avg,Lp}) + 0.22\ \mu_{EP,NL}^{(3)}\ (0.8\ E_{Avg,Lp}^3)} \quad (15)$$

**Fig. 3** illustrates predicted $|\mathbf{v}_{EK}|$ and $|\mathbf{v}_{EP,NL}^{(3)}|$ for particles P1 to P4 derived from empirical equations for Post1, Post2, and postless devices. The absolute values of the predicted $\mathbf{v}_{EP,NL}^{(3)}$ were plotted for better visualization, as all $\mu_{EP,NL}^{(3)}$ values are negative for all particles in this study. For particles P1 to P4, it is evident that $|\mathbf{v}_{EK}|$ is lowest in the postless device, with Post1 and Post2 showing almost equal values, although Post2 is slightly higher than Post1. This trend can be attributed to the combined influence of the electric fields $\mathbf{E}_{Avg,Ls}$ and $\mathbf{E}_{Avg,Lp}$ which contribute to a higher overall magnitude in the Post2 device compared to Post1, as detailed in **Table S7**. This indicates that the linear terms in the equations are device-dependent, with the postless device featuring nonintensified electric fields generating lower $|\mathbf{v}_{EK}|$ magnitudes. For all particles, it is apparent that the magnitude of $|\mathbf{v}_{EP,NL}^{(3)}|$ is the highest for Post1 device, and lowest for postless device. In the postless device, the uniform electric field distribution ensures a constant electric field throughout the entire migration channel at any applied voltage. In contrast, in Post devices, the presence of insulating features alters the electric field distribution, creating regions of higher field intensity. These localized high-intensity areas give rise to nonlinear electrokinetic phenomena, such as $EP_{NL}$. As reported in **Table S7**, $\mathbf{E}_{Avg,Lp}$ in the Post1 device is higher in magnitude compared to the Post2 device, while the postless device exhibits the lowest $\mathbf{E}_{Avg}$ among all the devices. The differences in the electric field distribution between the Post devices arise from variations in the insulating post dimensions, the vertical spacing (VS) between the insulating posts, the horizontal spacing (HS) between the posts, and length of the arms as reported in our previous studies.[24,27] In this case, the Post1 device, with a vertical spacing (VS) of 20 µm, intensifies the local electric field in the constrictions, while the Post2 device, with a VS of 35 µm and shorter arms, exhibits a less concentrated electric field in $L_p$ regions. The same trends for $\mathbf{v}_{EK}$ and $|\mathbf{v}_{EP,NL}^{(3)}|$ are observed for particles P5 to P8 shown in **Fig. S3**. These observations are consistent with previous reports from our group on improving iEK device design.[24,27]

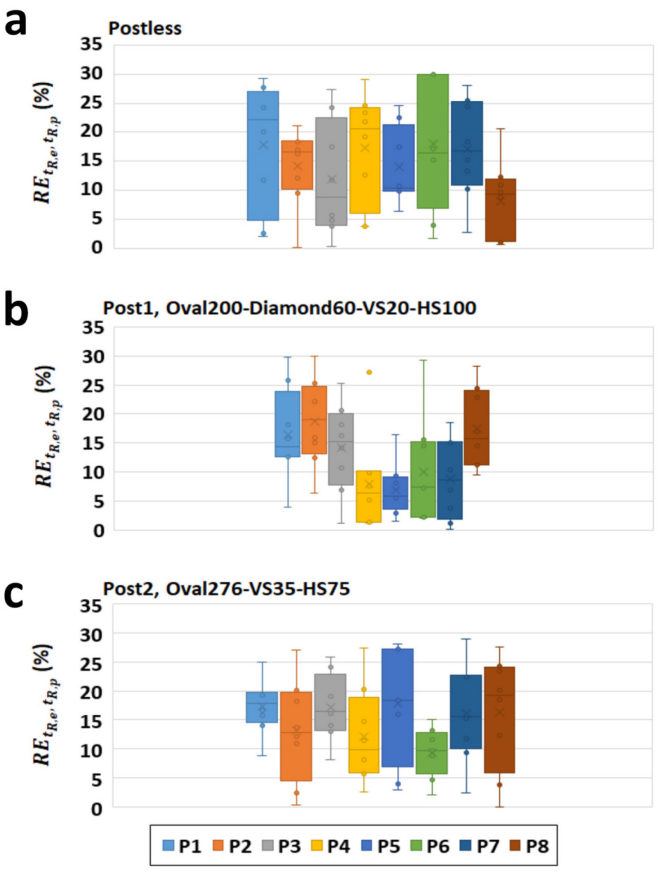


**Fig. 4** Box and Whisker plots representing relative error ($RE$) between $t_{R,p}$ and $t_{R,e}$ of the reference particles (P1–P8) across all applied voltages. Errors below 30% are considered acceptable. **(a)** postless device, **(b)** Post1 device and **(c)** Post2 device. All particles across three devices show $RE$ below 30%.

The average value for the weighting coefficient $A_1$, which corresponds to linear EK phenomena, in all three equations is 0.9 ± 0.3. This indicates that the corresponding variable or term contributes almost directly and proportionally to the outcome without requiring significant scaling or adjustment. This consistency demonstrates that the relationship between the variable and the response is neither excessively amplified nor diminished.

The main contributing factor to the observed $A_1$ value is the use of experimental linear mobilities ($\mu_{EP,L}$ and $\mu_{EO}$), which are derived under specific conditions where $\beta \ll 1$ and have very small magnitudes. These conditions ensure reliable and consistent experimental measurements of linear electrokinetic mobilities. The $A_1$ value close to 1 supports the validity of the experimental methodology and indicates that the electrokinetic term does not require further adjustment to reflect reality accurately.

The weighting coefficient $A_2$, which corresponds to nonlinear electrokinetic phenomena, is 1.32 for the postless device. This suggests that the uniform electric field distribution minimizes the

impact of nonlinear effects, as the term requires little adjustment to the governing equation. In contrast, for the Post1 and Post2 devices, A2 drops significantly to 0.32 and 0.22, respectively. These lower values indicate that the original equations substantially overestimate nonlinear contributions in the presence of posts. Assuming that $EP_{NL}$ primarily occurs in the regions between the posts (constrictions) where the electric field changes across the cutline, this observation can be attributed to the way that the electric field is calculated along the $L_p$ region. In this region, the electric field distribution is non-uniform. Since it is not feasible to use the electric field for each individual point, averaging the electric field values along the cutline ($E_{Avg,Lp}$) might affect the resolution of the calculations. In fact, there are points with maximum (or minimum) electric field values that are diminished (or increased) by averaging, thereby affecting their contribution to the overall nonlinear effect.

A further explanation for the observed $A_2$ value is the condition of elevated electric field values required to satisfy the cubic dependence necessary for experimentally calculating $\mu_{EP,NL}^{(3)}$. Compared to linear electrokinetic mobilities, $\mu_{EP,NL}^{(3)}$ is more challenging to determine and may be more prone to variability under these conditions. The results from the fitting process highlight that while the linear term remains dominant, the nonlinear term plays a role in determining the overall result.

Box and Whisker plots showing the relative error ($RE$) between $t_{R,e}$ and $t_{R,p}$ for the reference particles under all applied voltages are provided in **Fig. 4**. The plot illustrates the relative error $RE$ of reference particles (P1 to P8) across three device configurations: postless (**Fig. 4a**), Post1 (**Fig. 4b**), and Post2 (**Fig. 4c**). The boxplots display the median (central line), interquartile range (IQR; box bounds: 25th to 75th percentiles), and whiskers (extending to 1.5× IQR or min/max values). Outliers are shown as individual points. Errors below 30% are considered acceptable, signifying good agreement between experimental and predicted values. The 30% error threshold was chosen based on previous studies demonstrating that successful separations were achieved even when the discrepancy between predicted and experimental data reached approximately 30%.[20] Additionally, the literature[14,30] shows that large correction factors are often applied to improve the agreement between experimental and predicted results, which inevitably increases the error beyond 30%, suggesting that this threshold is a reasonable benchmark for our study. Across all three configurations, most particles exhibit $RE$ values within this acceptable range, demonstrating the reliable performance of the empirical equations for predicting particle retention times.

The $R^2$ for the derived equations (**Eqs. 13-15**) was approximately 0.8, which can be attributed to several factors. The main contributing factor to the observed $R^2$ is the way electric fields are incorporated into the solver. To simplify the model, average electric field values are used. However, the non-uniform nature of the electric field in post devices, complicates precise calculations. By averaging the electric field along the cutline, the method neglects extreme values—both maximum and minimum—masking their contribution to the overall influence. This oversimplification makes it difficult to determine electric field values with high accuracy.

Another factor affecting the $R^2$ value is the absence of an analytical model that accurately describes the experimental domain lying between the cubic model (where nonlinear velocity exhibits a cubic dependence on the electric field) and the 3/2 model (where nonlinear velocity follows a 3/2 dependence on the electric field). This gap in theoretical representation may contribute to the imperfect fit, as the existing models fail to fully capture the underlying physical or mathematical relationships governing the system. Despite these challenges, the derived equations remain consistent with the underlying physics of the system and provide an appropriate tool for predicting the retention time of particles in iEK systems.

## Comparison of predicted and experimental results for control particles

To validate the empirical equations, two control particles (P9 and P10) were selected based on their characteristics, which align with the reference particles in terms of size, zeta potential, and mobilities as detailed in **Table 1**. These particles were introduced into the microchannels using the EK injection method described in the previous section and tested across three device configurations—postless, Post1, and Post2—under four applied voltages (400 V, 700 V, 1000 V, 1300 V, and 1450 V). The retention times for these particles were predicted using the derived empirical equations (**Eqs. 13–15**) and compared to experimental results to assess the accuracy of the model. The experimental retention times ($t_{R,e}$), including standard deviations over three repetitions, and predicted retention times ($t_{R,p}$) for the control particles are presented in **Tables S8-S9**. Additionally, the percentage errors between the experimental and predicted values are provided in **Tables S8–S10**.

**Fig. 5** illustrates the comparison between $t_{R,p}$ and $t_{R,e}$ for particles P9 and P10 across the three device configurations and the applied voltages. In all cases, the retention times decreased as the applied voltage increased, reflecting the expected behavior of the system. For the postless device, the deviations between experimental and predicted retention times were below 23% for both P9 and P10 across all applied voltages, indicating a consistent performance of the empirical equation in a uniform electric field. For the Post1 and Post2 devices, the deviations were below 24% demonstrating the empirical equation's ability to effectively capture localized nonlinear effects of the electric field in this device.

Overall, the results demonstrate the reliability and accuracy of the empirical equations in predicting retention times under varying conditions. The relatively low deviations (below 24% in all cases) indicate that the equations fairly capture key factors influencing retention time, including both linear and nonlinear electrokinetic phenomena. Additionally, the trends observed in **Fig. 5** align with the theoretical expectations, further supporting the validity of the model. These findings confirm the empirical equations' potential for fairly predicting particle retention times across different microchannel designs and operational conditions.

 

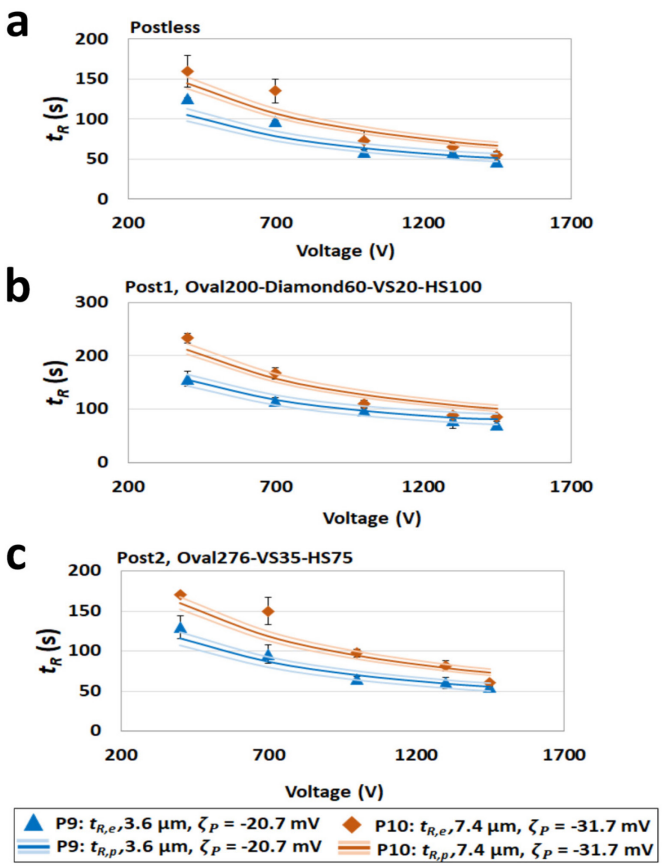


**Fig. 1** Comparison of the predicted retention time ($t_{R,p}$, solid lines) and experimental retention time ($t_{R,e}$, markers) as a function of applied voltage for control particles P9 (3.6 µm, $\zeta_P = -20.7\ mV$) and P10 (7.4 µm, $\zeta_P = -31.7\ mV$) across distinct three device configurations: **(a)** Postless, **(b)** Post1 (Oval200-Diamond60-VS20-HS100), and **(c)** Post2 (Oval276-VS35-HS75). Results are presented for four applied voltages (400 V, 700 V, 1000 V, 1300 V, and 1450 V). Confidence interval plots are included for the predicted retention time values.

## Conclusions

This study introduces a method for predicting particle retention time, accounting for both linear and nonlinear phenomena. The method combines particle characteristics, applied voltages, and microdevice design features. Using the collected experimental data, a set of empirical equations was developed to comprehensively describe the velocity of microparticles. These equations accounted for both electrokinetic and nonlinear velocity components, providing a reliable mathematical framework for predicting particle behavior under varying operational conditions. However, it is important to note that the model has limitations and is only applicable for predicting the retention time of particles within the provided range of particle characteristics. To validate the accuracy and reliability of the derived equations, two distinct control particles were tested across multiple device configurations. The validation results demonstrated good predictive capability, with prediction errors consistently remaining below 24% for all tested devices. This level of accuracy highlights the effectiveness of the empirical models in capturing the complex interplay of forces driving particle motion in electrokinetic systems. Potential strategies to further improve accuracy include refining the predictive model with advanced machine learning techniques and expanding the calibration dataset to capture broader experimental variability. Additionally, optimizing input parameters or reducing measurement noise in retention time data and mobilities could enhance precision beyond the current 20% error threshold.

These results underscore the potential of the proposed empirical equations in iEK systems for efficient prediction of particle behavior. To more thoroughly evaluate the nonlinear electrokinetic regime, future studies could focus on smaller particles that allow the use of higher electric fields without particle trapping, enabling a deeper exploration of the nonlinear velocity contribution. The method presented here offers significant advantages for advanced analytical applications, including enhanced accuracy, reduced processing time, and adaptability to diverse experimental conditions. By providing a reliable framework for modeling particle retention times, this study contributes to the advancement of microfluidic technologies, particularly in fields such as biomedical diagnostics, environmental monitoring, and chemical analysis, where precise control of particle behavior is critical.

## Author Contributions

Conceptualization, V.H.P.G and B.H.L.E.; methodology, V.H.P.G and B.H.L.E.; experimental data curation, A.V.K,; COMSOL simulations, A.V.K.,; writing—review and editing, A.V.K, V.H.P.G and B.H.L.E.; supervision, V.H.P.G and B.H.L.E.; project administration, V.H.P.G and B.H.L.E.; funding acquisition, B.H.L.E. All authors have read and agreed to the published version of the manuscript.

## Conflicts of interest

There are no conflicts to declare.

## Data availability

The data supporting this article have been included as part of the Supplementary Information.

## Acknowledgements

This material is based upon work supported by the National Science Foundation under Award No CBET- 2127592. The authors acknowledge Research Computing at the Rochester Institute of Technology for providing computational resources and support that have contributed to the research results reported in this publication. V.H.P.G. acknowledges the Federico Baur Endowed Chair in Nanotechnology (0020240I03) and the Nanotechnology and Semiconductors Research Group from Tecnologico de Monterrey. V.H.P.G. also acknowledges the financial support provided by the Consejo Nacional de Humanidades, Ciencia y Tecnología (SNI Grant 62382). A.V.K appreciates the helpful discussions provided by Carlos A. Mendiola-Escobedo, Viswateja Kasarabada, and Adrian Lomeli Martin during the development of this work.

## Notes and references

1 A. Vaghef-Koodehi and B. H. Lapizco-Encinas,

*Electrophoresis*, 2022, **43**, 263–287.

2 P. Rajapaksha, A. Elbourne, S. Gangadoo, R. Brown, D. Cozzolino and J. Chapman, *Analyst*, 2019, **144**, 396–411.

3 V. H. Perez-Gonzalez, *Electrophoresis*, 2021, **42**, 2445–2464.

4 B. H. Lapizco-Encinas, *Anal. Bioanal. Chem.*, 2022, 414, 885–905.

5 X. Xuan, *Electrophoresis*, 2022, 43, 167–189.

6 J. Ding, C. Woolley and M. A. Hayes, *Anal. Bioanal. Chem.*, 2017, **409**, 6405–6414.

7 P. V. Jones, G. L. Salmon and A. Ros, *Anal. Chem.*, 2017, **89**, 1531–1539.

8 M. Aghaamoo, A. Aghilinejad, X. Chen and J. Xu, *Electrophoresis*, 2019, **40**, 1486–1493.

9 C. V. Crowther, S. H. Hilton, L. K. Kemp and M. A. Hayes, *Anal. Chim. Acta*, 2019, **1068**, 41–51.

10 S. Soltanian-Zadeh, K. Kikkeri, A. N. Shajahan-Haq, J. Strobl, R. Clarke and M. Agah, *Electrophoresis*, 2017, **38**, 1988–1995.

11 V. Calero, P. Garcia-Sanchez, A. Ramos and H. Morgan, *Biomicrofluidics*, 2019, **13**, 054110.

12 J. Zhu and X. Xuan, *Biomicrofluidics*, 2011, **5**, 24111.

13 S. Patel, S. Qian and X. Xuan, *Electrophoresis*, 2013, **34**, 961–968.

14 N. Hill and B. H. Lapizco-Encinas, *Anal. Bioanal. Chem.*, 2020, **412**, 3891–3902.

15 A. S. Khair, *Curr. Opin. Colloid Interface Sci.*, 2022, 59, 101587.

16 M. Rouhi Youssefi and F. J. Diez, *Electrophoresis*, 2016, **37**, 692–698.

17 S. Tottori, K. Misiunas, U. F. Keyser and D. J. Bonthuis, *Phys. Rev. Lett.*, 2019, **123**, 14502.

18 F. A. Morrison, *J. Colloid Interface Sci.*, 1970, **34**, 210–214.

19 D. Li, in *Interface Science and Technology*, 2004, vol. 2, pp. 542–616.

20 A. Vaghef-Koodehi, C. Dillis and B. H. Lapizco-Encinas, *Anal. Chem.*, 2022, **94**, 6451–6456.

21 A. Vaghef-Koodehi, O. D. Ernst and B. H. Lapizco-Encinas, *Anal. Chem.*, 2023, **95**, 1409–1418.

22 V. Kasarabada, N. N. Nasir Ahamed, A. Vaghef-Koodehi, G. Martinez-Martinez and B. H. Lapizco-Encinas, *Anal. Chem.*, 2024, **96**, 15711–15719.

23 A. Vaghef-Koodehi and B. H. Lapizco-Encinas, *Biosens. 2024, Vol. 14, Page 119*, 2024, **14**, 119.

24 A. Vaghef-Koodehi, P. Cyr and B. H. Lapizco-Encinas, *J. Chromatogr. A*, 2024, **1722**, 464853.

25 N. N. Nasir Ahamed, C. A. Mendiola-Escobedo, V. H. Perez-Gonzalez and B. H. Lapizco-Encinas, *Micromachines*, , DOI:10.3390/mi14122239.

26 N. N. Nasir Ahamed, C. A. Mendiola-Escobedo, O. D. Ernst, V. H. Perez-Gonzalez and B. H. Lapizco-Encinas, *Anal. Chem.*, 2023, **95**, 9914–9923.

27 N. N. Nasir Ahamed, C. A. Mendiola-Escobedo, V. H. Perez-Gonzalez and B. H. Lapizco-Encinas, *Analyst*, 2024, **149**, 2469–2479.

28 N. N. Nasir Ahamed, C. A. Mendiola-Escobedo, V. H. Perez-Gonzalez and B. H. Lapizco-Encinas, *Biosensors*, 2024, **14**, 237.

29 D. A. Skoog, F. J. Holler and S. R. Crouch, *Principles of instrumental analysis*, CENGAGE Learning, Seventh ed., 2017, vol. 56.

30 H. Moncada-Hernandez, J. L. Baylon-Cardiel, V. H. Pérez-González and L.-E. H., *Electrophoresis*, 2011, **32**, 2502–2511.

31 B. Cardenas-Benitez, B. Jind, R. C. Gallo-Villanueva, S. O. Martinez-Chapa, B. H. Lapizco-Encinas and V. H. Perez-Gonzalez, *Anal. Chem.*, 2020, **92**, 12871–12879.

32 J. Bentor and X. Xuan, *Electrophoresis*, , DOI:10.1002/ELPS.202300188.

33 J. Bentor, H. Dort, R. A. Chitrao, Y. Zhang and X. Xuan, *Electrophoresis*, 2023, **44**, 938–946.

34 V. Kasarabada, O. D. Ernst, A. Vaghef-Koodehi and B. H. Lapizco-Encinas, *J. Chromatogr. A*, 2024, **1717**, 464685.

35 A. Coll De Peña, A. Miller, C. J. Lentz, N. Hill, A. Parthasarathy, A. O. Hudson and B. H. Lapizco-Encinas, *Anal. Bioanal. Chem.*, 2020, **412**, 3935–3945.

36 M. A. Saucedo-Espinosa, A. Lalonde, A. Gencoglu, M. F. Romero-Creel, J. R. Dolas and B. H. Lapizco-Encinas, *Electrophoresis*, 2016, **37**, 282–290.

37 M. A. Saucedo-Espinosa and B. H. Lapizco-Encinas, *Biomicrofluidics*, 2016, **10**, 033104.

38 O. D. Ernst, A. Vaghef-Koodehi, C. Dillis, A. Lomeli-Martin and B. H. Lapizco-Encinas, *Anal. Chem.*, 2023, **95**, 6595–6602.

39 A. Lomeli-Martin, O. D. Ernst, B. Cardenas-Benitez, R. Cobos, A. S. Khair and B. H. Lapizco-Encinas, *Anal. Chem.*, 2023, **95**, 6740–6747.

40 J. M. de los Santos-Ramirez, C. A. Mendiola-Escobedo, J. M. Cotera-Sarabia, R. C. Gallo-Villanueva, R. Martinez-Duarte and V. H. Perez-Gonzalez, *Analyst*, , DOI:10.1039/d4an00538d.

 